# Ultrathin MXene-Micropattern-Based Field-Effect Transistor for Probing Neural Activity

*Bingzhe Xu, Minshen Zhu, Wencong Zhang, Xu Zhen, Zengxia Pei, Qi Xue, Chunyi Zhi,* and Peng Shi**

MXenes, a new family of 2D materials, combine hydrophilic surface with metallic conductivity.[1–7] Since the introduction in 2011,[6] MXene's excellent mechanical, electrical, chemical, and physical properties have sparked great interests in exploiting MXenes for energy storage,[8–14] nanocomposite fabrication,[7,15,16] and chemical sensing.[17–19] However, despite the great potential of creating MXene-based biosensing devices,[3,18] there is still no report demonstrating the use of MXene for probing cellular functions in a biologically relevant context. With a hydrophilic surface property and 2D layered atomic structures, MXene could be a promising candidate to create biologically compatible[18] field-effect transistors (FET) for rapid, straightforward, and label-free detection of biological events. Notably, MXenes can be easily micromachined to accommodate various geometries with large contact surfaces. This property can greatly simplify device manufacturing procedures, which would otherwise require complicated processes (e.g., chemical vapor deposition, epitaxial growth or mechanical exfoliation). These methods are either low-yield or high-cost, and have been used for FET devices based on other materials such as carbon nanotubes,[20,21] nanowires[22,23] or graphene.[24–28]

Here, we developed a simple and effective technique for fabricating FET transistors based on ultrathin conductive $Ti_3C_2$-MXene micropatterns, which were utilized to perform highly sensitive label-free detection of dopamine, as well as to monitor spiking activity in hippocampal neurons. The MXene-FET biosensor was well compatible with long term neuronal culture. The transparent ultrathin (≈5 nm) layer of $Ti_3C_2$-MXene micropatterns had no interference with traditional microscpy, so that calcium imaing of neural activity could be simultaneoulsy conducted with electrical measurement using the MXene-FET with a temporal resolution of ≈50 ms. To our best knowledge, this study is the first demonstration of using MXenes for probing biological events in a cellular model. The straightforward method for fabricating the MXene–FET biosensors would also facilitate the adoption of this technique in a wide range of biomedical applications.

$Ti_3C_2$–MXene was synthesized by selectively etching the Al layer in precursor material $Ti_3AlC_2$ with 48% hydrofluoric acid (HF). The resulted bulk MXenes ($Ti_3C_2T_x$) were firstly examined by scanning electron microscopy (SEM) to confirm the multilayered structure (**Figure 1**a). X-ray diffraction (XRD) was also used to analyze the chemical composition of the fabricated MXene, showing the transformation from $Ti_3AlC_2$ to $Ti_3C_2T_x$ (Figure 1b). The most intense peak at 39° of $Ti_3AlC_2$ disappeared after etching treatment, indicating the removal of Al layer. In addition, the (00*l*) peaks of $Ti_3C_2T_x$, such as (002) at 9.5° and (004) at 19.4°, broadened with less intensity and shifted to lower angles (8.8° and 18.5°, respectively), indicating Al was replaced by —OH or —F moieties. After being intercalated in dimethyl sulfoxide (DMSO) and delaminated via sonication, few and single layer of MXene flakes are ready for patterning and sensing applications (Figure 1c).

The ultrathin MXene micropatterns were created by microcontact printing (μCP), as shown in **Figure 2**a. MXene dispersed in aqueous solution was used to ink PDMS stamps with patterns of alternating grooves (20 μm) and ridges (20 μm), which was then printed onto 3-aminopropyltriethoxysilane (APTES, Sigma-Aldrich) modified coverslips. After removal of the stamps, one or several layers of MXene stripes were left on the coverslips. These MXene stripes provide an active surface to bind small biomolecules, which in turn change the conductivity of the ultrathin MXene stripes. The highly sensitive response to electrochemical perturbation makes MXene a good candidate for biosensing applications (Figure 1c). As shown in Figure 2b, this μCP-based method could consistently create large-scale uniform MXene micropatterns. The width of MXene stripes was selected as 20 μm to ensure high electrical conductance as well as large surface area to interact with biomolecules. The thickness of micropatterns was regulated by controlling the concentration of MXene ink, which was set to create micropatterns of ≈5 nm as shown in Figure 2c. Also, the micropatterns did not show any dramatic variations in topography, indicating the high quality of our printing process. Even though thinner MXene stripes could also be achieved by μCP, too diluted MXene ink would cause discontinuity in the resulted micropatterns, and thus failure of the final sensing device.

B. Xu, W. Zhang, X. Zhen, Dr. P. Shi
Department of Mechanical and Biomedical Engineering
City University of Hong Kong
83 Tat Chee Ave
Kowloon, Hong Kong SAR 999077, P. R. China
E-mail: pengshi@cityu.edu.hk

M. Zhu, Z. Pei, Q. Xue, Dr. C. Zhi
Department of Physics and Material Science
City University of Hong Kong
83 Tat Chee Ave
Kowloon, Hong Kong SAR 999077, P. R. China
E-mail: cy.zhi@cityu.edu.hk

Dr. P. Shi
Shenzhen Research Institute
City University of Hong Kong
Shenzhen 518057, P. R. China

**DOI: 10.1002/adma.201504657**

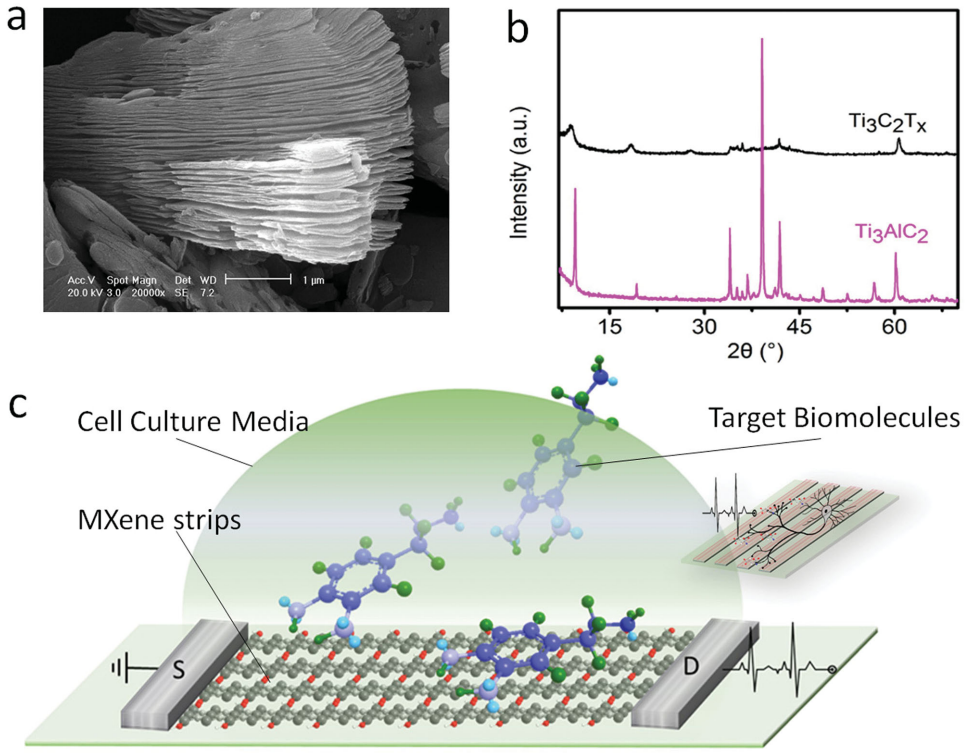


**Figure 1.** Characterization of bulk MXene. a) SEM image of the multilayer-structured MXene. b) XRD patterns of the transition from $Ti_3AlC_2$ to $Ti_3C_2T_x$. c) Schematic of a biosensing device based on MXene field-effect transistors.

To characterize the electrical properties of MXene micropatterns, a pair of silver electrodes was deposited orthogonally to the strips with gap distances ranging from 2 to 10 mm. As shown in **Figure 3**a, these MXene strips were electrically continuous and followed the Ohm's law exhibiting a linear relationship between voltages and currents. This result indicated a stable conductance of the MXene stripe without gating control. The lengths of MXene stripes were also observed to be linearly related to the device's resistance (conductance) (Figure 3b), suggesting that conductance of the device was mostly determined by the properties of MXene micropatterns.

Then we explored whether the electrical access of MXene micropatterns could be altered by different gating controls. A solution-gated MXene device was set up as shown in Figure 3c. The source and drain electrodes were made by high purity sliver painted orthogonal to MXene stripes with a gap distance of 1 cm. Insulation between the electrodes and the bath solution was achieved by a PDMS chamber, preventing current leakage from the electrodes. A gate voltage was applied through an Ag/AgCl electrode immersed in the bath solution. As shown in Figure 3d, the conductance of the device can be modulated by applying different gate voltages, and a V-shaped ambipolar field-effect characteristic was observed. Similar V-shape feature has also been observed in graphene FET devices.[29,30] The MXene-based device acted as an n-type FET when gate voltage was above +0.3 V, and became p-type mode when gate potential level was below +0.3 V. These results proved that the fabricated MXene device showed an apparent field-effect response to front-gate modulation and the semiconductive characterization made it a suitable material for biosensing applications.

As a proof-of-concept study, the MXene-micropattern-based FET device was used to detect a small biological molecule, dopamine, which is a typical neurotransmitter involved in regulating many brain functions.[31–33] It has been reported that dopamine molecules can strongly interact with free electrons in the functional terminals on graphene surfaces (e.g., —OH) through $\pi$–$\pi$ interaction, causing doping effect.[34–36] Similarly, dopamine molecules could also interact with electrons from the terminal groups (e.g., —OH or —F) on MXene surfaces, resulting in an increase in the number of holes, and enhancing the conductance. The device was composed of two major elements: a biosensing compartment and a transistor circuit for electrical measurement. The amount of pulse-released dopamine in the biosensing chamber was precisely controlled by using a microinjector on the femto-liter resolution (**Figure 4**a). In this experiment, the FET was operated in the p-channel mode. When dopamine molecules were released to interact with the MXene surface, changes in the conductance of the FET device could be measured in real-time to reflect the binding events (Figure 4b). When the dopamine concentration was raised from 0 to $2 \times 10^{-3}$ M in the sensing compartment, the device conductance changed by over 20% with obvious modulation upon pulsed dopamine release by microinjection (Figure 4c,d), and the lowest detection limit was as low as $100 \times 10^{-9}$ M. The increase of the conductance was gradually saturated when dopamine concentration reached $2 \times 10^{-3}$ M and above (Figure 4d). Over a large range of dopamine concentrations, from $100 \times 10^{-9}$ M to $50 \times 10^{-6}$ M, the device conductance also showed highly linear modulation ($R^2 = 0.9994$, Figure 4 insert), further highlighting its potential for quantitative detection of biological molecules.

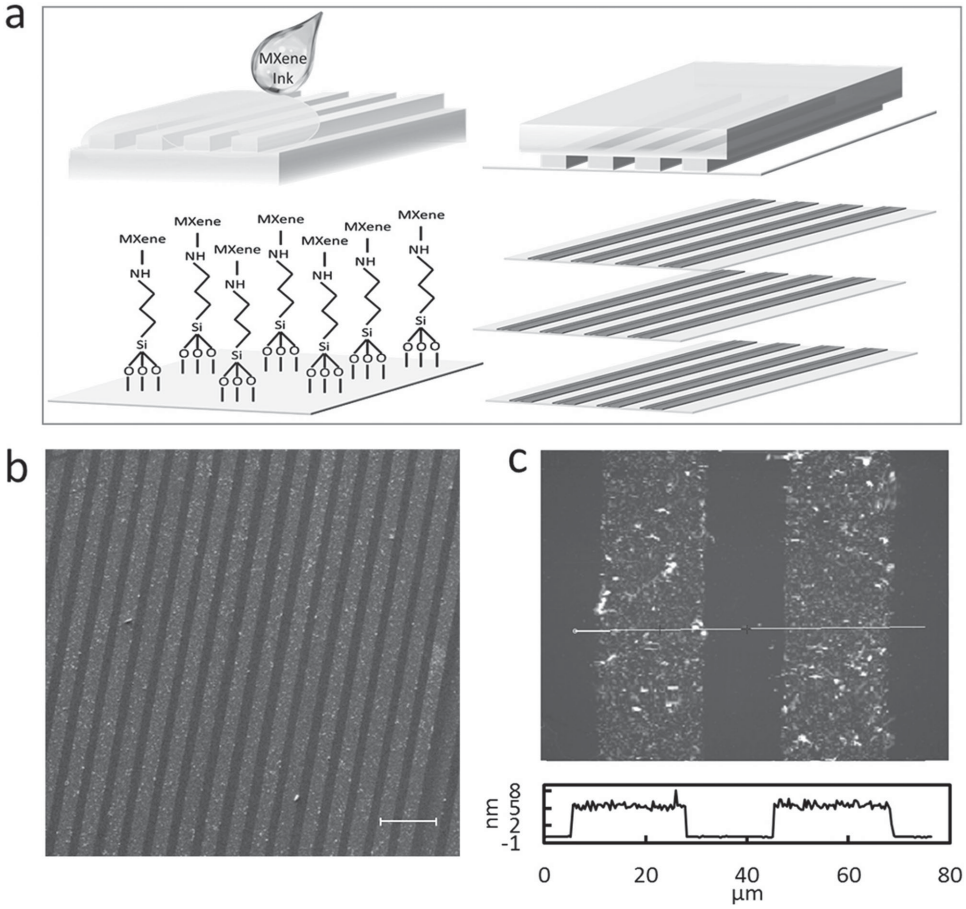


**Figure 2.** Micropattering of MXene on glass substrates. a) Illustration of the patterning process by using μCP. b) SEM image of a substrate patterned with MXene stripes. Scale bar, 100 μm. c) AFM image for analyzing the height of MXene micropatterns.

As the release of neurotransmitters is usually a result of action potential firing,[37] we then used the MXene-based FET device to achieve real-time monitoring of spiking activity in cultured primary hippocampal neurons (**Figure 5**a). The MXene material showed a very good biocompatibility with MXenes even in long term cultures. Before seeding neurons, the substrates with MXene micropatterns were briefly coated with poly-L-lysine and laminin to enhance the adhesion of neuron cells. As shown in Figure 5b, neurons showed normal morphology with elaborated neurites on the MXene micropatterned substrates. The 5 nm MXene patterns did not induce any edge effects in neuronal cultures, as the neurite outgrowth was quite random as shown in Movie S1 in the Supporting Information. At 7–8 d in vitro (DIV), medium with high $K^+$ concentration were used to stimulate the primary neurons in the culture; and electrical measurement (currents from source to drain) and calcium imaging were performed simultaneously to verify the capability of our MXene-based FET device for capturing neural activity in real-time. Due to the ultrathin thickness (≈5 nm) of the MXene micropatterns, the device was nearly transparent (Figure 5b), so that traditional microscopic observation was not interfered. Comparing current recordings with calcium signals, the current fluctuation shared great similarity with the fluorescence changes as reported by Fluo4-AM (Figure 5c, Movie S1, Supporting Information). The spike trains (series of action potentials) derived from electrical and optical recording showed a very high correlation coefficient of 0.82. The MXene device showed great temporal resolution, as it captured spikes that were not observable in calcium imaging due to the slow dynamics (on the order of hundred milliseconds) of calcium signaling in neuron cells. Even though a slight decrease in conductivity of our $Ti_3C_2$–MXene–FET was observed over the experiment window (7–8 d), it did not greatly affect the biosensing performance of the device, and is probably due to slow oxidation of $Ti_3C_2$ in culture medium.[38] The results directly associated electrical measurements (by MXene–FET) with the onset of action potentials (recorded by calcium imaging), and clearly demonstrate the capability of the MXene-based biosensor for real-time monitoring of neural activities.

In this study, we developed a highly sensitive device based on $Ti_3C_2$–MXene–FET for detecting neurotransmitters, and for probing action potentials in primary hippocampal neurons. To our best knowledge, this is the first time an MXene has been nanopatterned, and also the first experimental report on an MXene sensor for probing neural activity. Functionally, the device could detect dopamine at a concentration as low as $100 \times 10^{-9}$ M, which is already dramatically lower than many previously published results using graphene-based

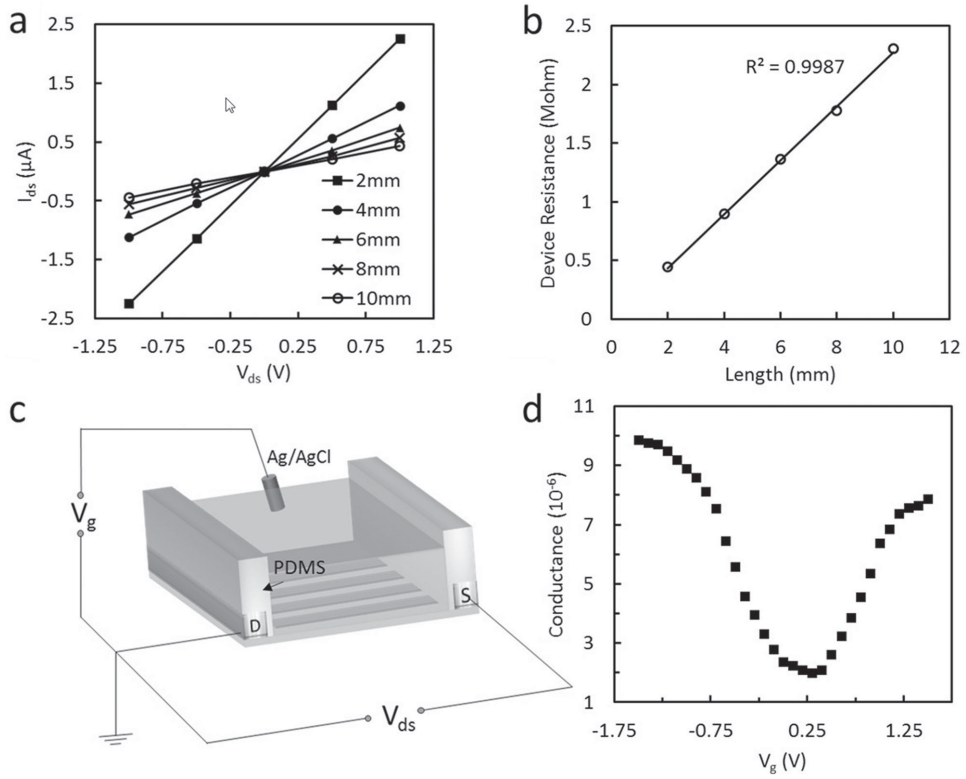


**Figure 3.** Electrical characterization of MXene micropatterns. a) Current/voltage curves at $V_{ds}$ varying from −1 to 1 V on MXene strips of different lengths (2, 4, 6, 8, 10 mm). b) Analysis of the relationship between the resistances and the lengths of MXene stripe patterns. c) Schematic of the experimental setup of the MXene–FET device using a solution gate. d) Analysis of the V-shaped ambipolar field-effect characteristic of a device based on MXene micropatterns.

biosensors.[39–43] In the proof-of-concept experiments, the core components of the MXene–FET were micropatterns created by μCP. The optimal parameters of the micropatterns, including thickness, width, length, and ink concentration, can potentially be further tuned to improve the performance of the devices.

Even though pure $Ti_3C_2T_x$ has been predicted to be metallic by density functional theory,[3] it has been reported that surface termination can be tuned to render the material semiconductor property.[44,45] Especially for $Ti_3C_2$ prepared by exfoliation of $Ti_3AlC_2$ in HF, the surface is likely to be functionalized with hydroxyl (—OH) and/or fluorine (—F) groups, which could turn the derivative material to semiconductor with narrow bandgaps (Figure S1, Supporting Information).[44,45] Unlike graphene with a zero-bandgap, a proper bandgap with MXenes reduces current leakages in an off state,[46] and therefore helps to achieve better detection sensitivity in our devices. The detection limit could potentially be further improved by tuning the micropattern properties and the transistor circuits.

The material, MXenes, also exhibited excellent biocompatibility, as reflected by our long-term culture of primary hippocampal neurons on the devices. It is well known that primary neurons are extremely fragile and hard to culture,[47] we showed well elaborated neuronal growth on MXene micropatterns, and further established MXene's compatibility with delicate biological systems. These features guaranteed good interfacing of neuron cells with the electronic components in the system, which enabled real-time, label-free monitoring of neuronal spiking activities. Meanwhile, the transparent ultrathin (≈5 nm) layer of MXene micropatterns did not interfere with traditional optical microscopic observation of the cells, so that calcium imaging for neural activity could be simultaneously conducted and compared with electrical measurement using MXene–FET. It was found that the MXene–FET actually achieved a much better temporal resolution than the widely used calcium sensitive dye (Fluo-4). Besides the functional advantages, the extraordinary machinability of MXene and a μCP-based fabrication process provide a cost-effective solution for potential scaleup production of biodevices compared with graphene and CNTs, which render MXene a great economic advantage for industrial production.

## Experimental Section

*Preparation and Characterization of MXene*: $Ti_3AlC_2$ (1 g) power was immersed in 10 mL 48% HF, and stirred for 20 h at room temperature. The obtained powder was then rinsed multiple times with deionized water. The powder pellet was retrieved by centrifugation at 3500 rpm for 10 min, and the supernatant was discarded. The final product ($Ti_3C_2T_x$ powder) was dried at 80 °C under vacuum for 12 h. In an $N_2$-protected environment, the $Ti_3C_2T_x$ powder was then placed in 10 mL DMSO, and stirred for 18 h. The DMSO was removed by centrifugation at 3500 rpm for 5 min. The intercalated $Ti_3C_2T_x$ was then dispersed in deaerated water ($Ti_3C_2T_x$:water = 1:300, mass ratio) and sonicated for 5 h under the protection of $N_2$. The MXene–water mixture was then centrifuged at 1000 rpm for 2 h, and the supernatant was collected for further experiments.

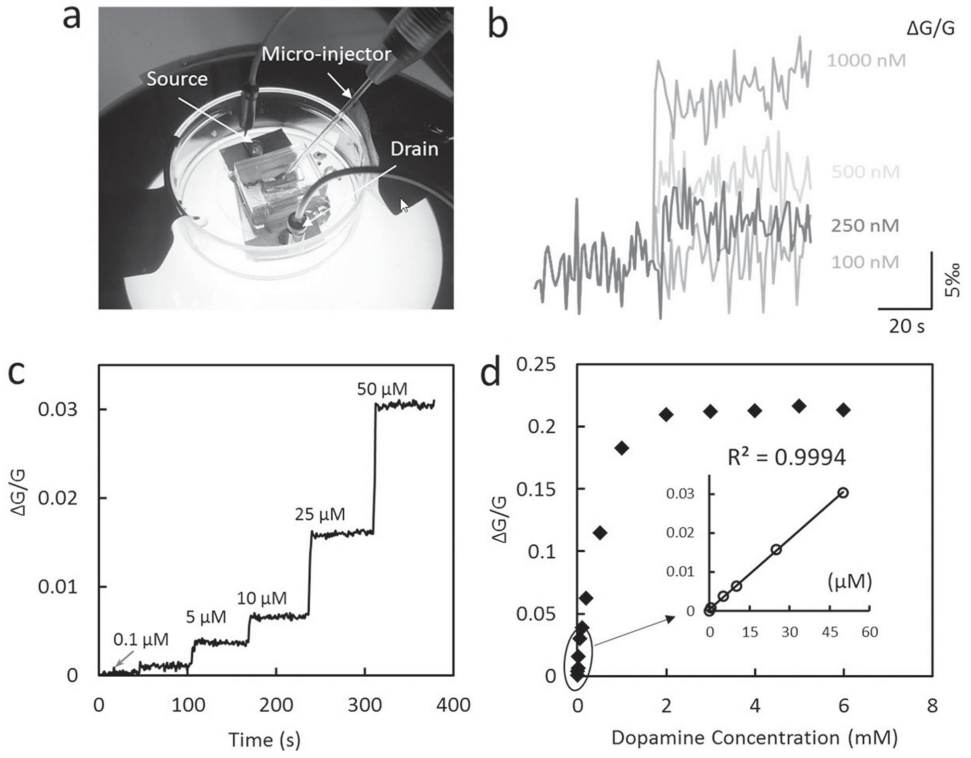


**Figure 4.** Dopamine sensing with the MXene–FET device. a) Photograph showing the MXene–FET device coupled with a microinjector for precisely controlled pulsed releasing of dopamine in the biosensing chamber. b) Recordings of the conductivity variation of the MXene device upon addition of 100, 250, 500, $1000 \times 10^{-9}$ M dopamine. c) Real-time monitoring of conductivity fluctuations of an MXene device for dopamine concentrations varying from $100 \times 10^{-9}$ M to $50 \times 10^{-6}$ M. d) Analysis of the dopamine detection range of the MXene–FET devices. The inset shows a highly linear modulation of the device conductivity for dopamine concentrations from $100 \times 10^{-9}$ M to $50 \times 10^{-6}$ M.

The morphologies of the sample were examined by an environmental scanning electron microscope (FEI/Philips XL30). The crystallographic characteristics were analyzed by powder X-Ray Diffraction using a Bruker D2 Phaser diffractometer, equipped with Cu K$\alpha$ radiation ($\lambda = 1.54$ Å).

*MXene Micropatterning and Characterization*: Coverslips (Bellco Glass, Germany) were cleaned in piranha solution ($H_2SO_4$:$H_2O_2$ = 7:3) at 120 °C for 2 h, followed by extensive rinse using deionized water. The coverslips were then treated with 1% APTES in acetone, and dried with $N_2$ for the following stamping procedure. A polydimethylsiloxane (PDMS) stamp was fabricated by replica-molding from a negative silicon master with strip features of 20 μm width and 1 cm length. After plasma-treatment for 5 min, the stamps were uniformly covered with a thin layer of the MXene ink and dried in a vacuum. The MXene-coated PDMS stamp was then gently applied on a coverslip for 3–5 min. Upon removal of the stamp, micropatterns of several layers of MXene were formed on the glass substrates.

The MXene micropatterns were examined by using SEM (FEI Quanta 250 Environment), and then by atomic force microscopy (AFM, Bruker Dimension Icon) in a peaking force mode with a silicon tip (resonant frequency, 70 kHz; spring constant, 0.4 N $m^{-1}$).

*Electrical Characterization*: The Electrical properties of the MXene devices were analyzed with a sourcemeter (Keithley, 2614B). A pair of silver electrodes was deposited orthogonal to the strips with gap distances ranging from 2 to 10 mm and a PDMS chamber was built to insulate the silver electrodes from the inside electrolyte solution, which contains $10 \times 10^{-3}$ M HEPES, $140 \times 10^{-3}$ M NaCl, $1 \times 10^{-3}$ M $MgCl_2$, $5.5 \times 10^{-3}$ M KCl, and $2 \times 10^{-3}$ M $CaCl_2$ @ pH 7.2. For characterization of the FET properties on the MXene device, the source–drain electrodes potential range was biased at 1 V.

*Cell Culture*: All procedures involving animals were approved by the animal ethical committee of the City University of Hong Kong. Before use, the final MXene–FET devices were placed in 70% ethanol solution overnight for sterilization. Hippocampal neurons were cultured on pre-assembled MXene devices. The device substrates were coated with polylysine (Sigma) at 100 μg $mL^{-1}$ overnight and then laminin at 10 μg $mL^{-1}$ (Life Technology) for 4 h before seeding neuron cells. Hippocampi tissue were dissected from E18 embryonic Sprague Dawley rats, and treated with papain (Sigma) for 30 min at 37 °C. Dissociated neurons were prepared by triturating enzymatic treated tissue with a 1 mL pipette tip in Dulbecco's modified Eagle's medium containing 10% fetal bovine serum. Neurons were then seeded onto coated MXene devices at a density of $3–5 \times 10^4$ $cm^{-2}$. After the initial adhesion of neuron cells (2 h after seeding), the medium was replaced by Neurobasal medium supplemented with B27, L-glutamine and penicillin/streptomycin. Half of the medium was replaced with fresh medium every 3–4 d.

*Detection of Neural Activity*: For dopamine detection, the source–drain current ($I_{ds}$) was continuously recorded with a bias voltage of 1 V, while dopamine concentration was precisely and gradually increased by using a digital microinjector (Sutter, XenoWorks). The fluctuation in the device conductance was calculated to indicate the dopamine releasing events. For monitoring neuronal spiking activity, neurons were cultured for one week before use. The fluctuation of the $I_{ds}$ was measured in parallel with calcium imaging on an inverted microscope equipped with a 10× objective (IX81, Olympus). The $K^+$ concentration was increased to $25 \times 10^{-3}$ M to increase the spontaneous firing in the neuron cells.

*Calcium Imaging*: A stock solution of the calcium sensitive dye Fluo4-AM (Life Technologies) at $1.5 \times 10^{-3}$ M was prepared in DMSO and further diluted in artificial cerebrospinalfluid (ACSF) solution ($126 \times 10^{-3}$ M NaCl, $3 \times 10^{-3}$ M KCl, $26 \times 10^{-3}$ M $NaHCO_3$, $1 \times 10^{-3}$ M $NaH_2PO_4$, $2 \times 10^{-3}$ M $CaCl_2$, $1 \times 10^{-3}$ M $MgSO_4$, $10 \times 10^{-3}$ M dextrose) to a final concentration of $2 \times 10^{-6}$ M. The neurons were then incubated with Fluo-4 AM for 30 min at room temperature in the dark before

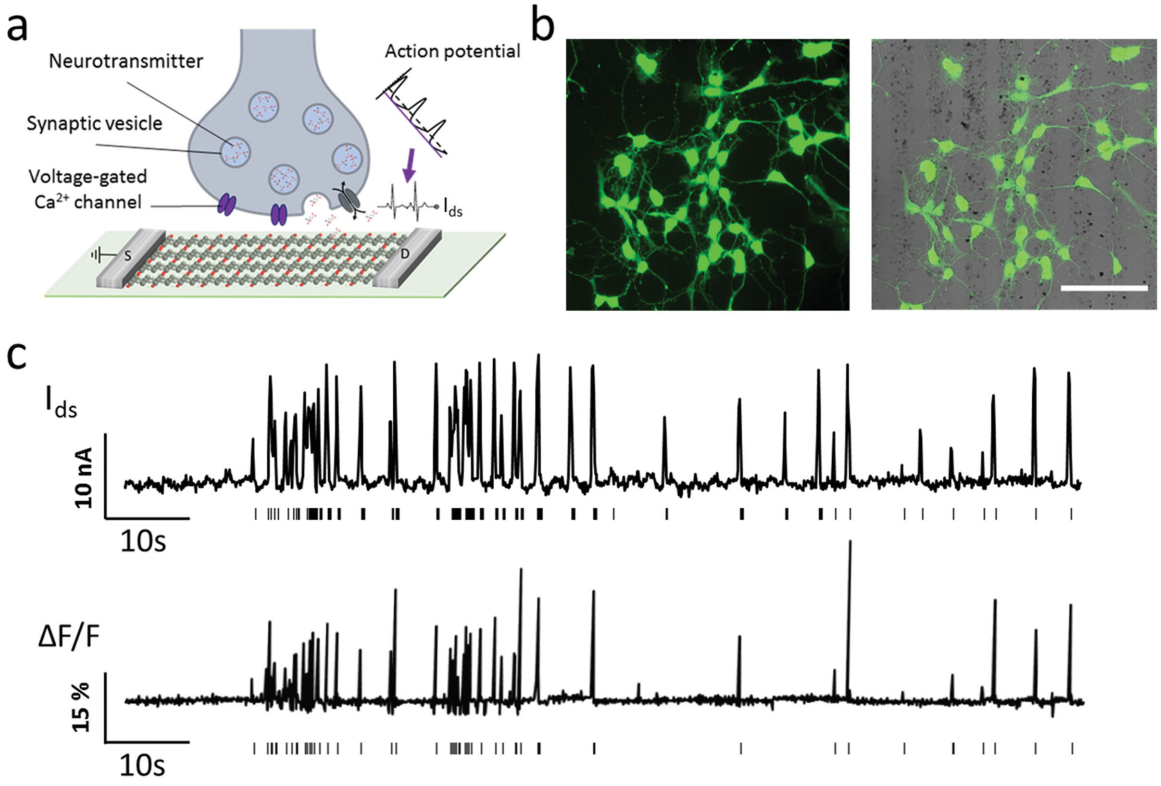


**Figure 5.** Real-time monitoring of spiking activities in primary neurons. a) Schematic showing the working principle of probing action potential by using the MXene–FET device. Upon the firing of action potentials, neurotransmitters are released, which subsequently bind to the MXene surface to induce fluctuation of electrical signals. b) Left panel: Fluorescence image of neurons immunostained for *βIII*-tubulin. Right panel: Merged image combining the bright-field and fluorescence channels to show good compatibility between the neuron cells and the MXene micropattern. Scale bar, 100 μm. c) The derivation of neuronal spiking activities by using current measurements with the MXene–FET device. The results were confirmed by and compared to recordings obtained with simultaneously conducted calcium imaging (using the Fluo-4 probe).

imaging. Excessive dye molecules were removed by gently rinsing the neurons three to four times with fresh ACSF solution. The sample was then mounted on an inverted microscope. To analyze the calcium imaging results, the fluorescence change over time was defined as $\Delta F/F_0 = (F_1–F_0)/F_0$, where $F_1$ indicated the fluorescence intensity of a current frame and $F_0$ indicated the fluorescence intensity of the previous frame. The spike trains were derived by thresholding the $\Delta F/F_0$ curve.

*Immunocytochemistry*: For analysis, cells were fixed for 30 min in 4% paraformaldehyde in phosphate-buffered saline (PBS), permeablized in 0.25% Triton X-100 for 15 min, and then blocked with 4% bovine serum albumin (BSA) in PBS for 2 h at room temperature or overnight at 4 °C. Samples were incubated with primary antibodies (anti-βIII tubulin, Millipore) in 4% BSA for 2 h at room temperature, rinsed with PBS, incubated with secondary antibodies for 1 h, and were again rinsed with PBS.

## Supporting Information

Supporting Information is available from the Wiley Online Library or from the author.

## Acknowledgements

B.X. and M.Z. contributed equally to this work. This work was supported by the National Natural Science Foundation of China (NSFC81201164), Early Career Scheme from RGC Hong Kong (ECS125012), General Research Fund from RGC Hong Kong (GRF11211314, GRF11218015), Innovation and Technology Commission of Hong Kong (ITS/376/13), and grants from the City University of Hong Kong (ARG9667120).

Received: September 21, 2015
Revised: November 9, 2015
Published online: February 29, 2016

[1] M. Naguib, Y. Gogotsi, *Acc. Chem. Res.* **2014**, *48*, 128.
[2] J.-C. Lei, X. Zhang, Z. Zhou, *Front. Phys.* **2015**, *10*, 276.
[3] M. Naguib, V. N. Mochalin, M. W. Barsoum, Y. Gogotsi, *Adv. Mater.* **2014**, *26*, 992.
[4] M. Naguib, O. Mashtalir, J. Carle, V. Presser, J. Lu, L. Hultman, Y. Gogotsi, M. W. Barsoum, *ACS Nano* **2012**, *6*, 1322.
[5] M. Naguib, J. Halim, J. Lu, K. M. Cook, L. Hultman, Y. Gogotsi, M. W. Barsoum, *J. Am. Chem. Soc.* **2013**, *135*, 15966.
[6] M. Naguib, M. Kurtoglu, V. Presser, J. Lu, J. Niu, M. Heon, L. Hultman, Y. Gogotsi, M. W. Barsoum, *Adv. Mater.* **2011**, *23*, 4248.
[7] M.-Q. Zhao, C. E. Ren, Z. Ling, M. R. Lukatskaya, C. Zhang, K. L. Van Aken, M. W. Barsoum, Y. Gogotsi, *Adv. Mater.* **2015**, *27*, 339.
[8] D. Er, J. Li, M. Naguib, Y. Gogotsi, V. B. Shenoy, *ACS Appl. Mater. Interfaces* **2014**, *6*, 11173.
[9] M. Naguib, J. Come, B. Dyatkin, V. Presser, P.-L. Taberna, P. Simon, M. W. Barsoum, Y. Gogotsi, *Electrochem. Commun.* **2012**, *16*, 61.
[10] M. R. Lukatskaya, O. Mashtalir, C. E. Ren, Y. Dall'Agnese, P. Rozier, P. L. Taberna, M. Naguib, P. Simon, M. W. Barsoum, Y. Gogotsi, *Science* **2013**, *341*, 1502.

[11] D. Sun, M. Wang, Z. Li, G. Fan, L.-Z. Fan, A. Zhou, *Electrochem. Commun.* **2014**, *47*, 80.
[12] Q. Tang, Z. Zhou, P. Shen, *J. Am. Chem. Soc.* **2012**, *134*, 16909.
[13] Y. Xie, Y. Dall'Agnese, M. Naguib, Y. Gogotsi, M. W. Barsoum, H. L. Zhuang, P. R. C. Kent, *ACS Nano* **2014**, *8*, 9606.
[14] Y. Xie, M. Naguib, V. N. Mochalin, M. W. Barsoum, Y. Gogotsi, X. Yu, K.-W. Nam, X.-Q. Yang, A. I. Kolesnikov, P. R. C. Kent, *J. Am. Chem. Soc.* **2014**, *136*, 6385.
[15] X. Liang, A. Garsuch, L. F. Nazar, *Angew. Chem. Int. Ed.* **2015**, *54*, 3907.
[16] Z. Ling, C. E. Ren, M.-Q. Zhao, J. Yang, J. M. Giammarco, J. Qiu, M. W. Barsoum, Y. Gogotsi, *Proc. Natl. Acad. Sci. USA* **2014**, *111*, 16676.
[17] X.-f. Yu, Y.-c. Li, J.-b. Cheng, Z.-b. Liu, Q.-z. Li, W.-z. Li, X. Yang, B. Xiao, *ACS Appl. Mater. Interfaces* **2015**, *7*, 13707.
[18] H. Liu, C. Duan, C. Yang, W. Shen, F. Wang, Z. Zhu, *Sens. Actuators B: Chem.* **2015**, *218*, 60.
[19] F. Wang, C. Yang, M. Duan, Y. Tang, J. Zhu, *Biosens. Bioelectron.* **2015**, *74*, 1022.
[20] J. A. Misewich, R. Martel, P. Avouris, J. C. Tsang, S. Heinze, J. Tersoff, *Science* **2003**, *300*, 783.
[21] A. Javey, J. Guo, Q. Wang, M. Lundstrom, H. Dai, *Nature* **2003**, *424*, 654.
[22] L. J. Lauhon, M. S. Gudiksen, D. Wang, C. M. Lieber, *Nature* **2002**, *420*, 57.
[23] Y. Cui, Q. Wei, H. Park, C. M. Lieber, *Science* **2001**, *293*, 1289.
[24] X. Dong, Y. Shi, W. Huang, P. Chen, L. J. Li, *Adv. Mater.* **2010**, *22*, 1649.
[25] D. Khatayevich, T. Page, C. Gresswell, Y. Hayamizu, W. Grady, M. Sarikaya, *Small* **2014**, *10*, 1505.
[26] G. Xu, J. Abbott, L. Qin, K. Y. Yeung, Y. Song, H. Yoon, J. Kong, D. Ham, *Nat. Commun.* **2014**, *5*, 4866.
[27] S. Mao, G. Lu, K. Yu, Z. Bo, J. Chen, *Adv. Mater.* **2010**, *22*, 3521.
[28] M. Dankerl, M. V. Hauf, A. Lippert, L. H. Hess, S. Birner, I. D. Sharp, A. Mahmood, P. Mallet, J. Y. Veuillen, M. Stutzmann, J. A. Garrido, *Adv. Funct. Mater.* **2010**, *20*, 3117.
[29] I. Meric, M. Y. Han, A. F. Young, B. Ozyilmaz, P. Kim, K. L. Shepard, *Nat. Nanotechnol.* **2008**, *3*, 654.
[30] Z. Liu, L. Ma, G. Shi, W. Zhou, Y. Gong, S. Lei, X. Yang, J. Zhang, J. Yu, K. P. Hackenberg, A. Babakhani, J.-C. Idrobo, R. Vajtai, J. Lou, P. M. Ajayan, *Nat. Nanotechnol.* **2013**, *8*, 119.
[31] John D. Salamone, M. Correa, *Neuron* **2012**, *76*, 470.
[32] A. Usiello, J.-H. Baik, F. Rouge-Pont, R. Picetti, A. Dierich, M. LeMeur, P. V. Piazza, E. Borrelli, *Nature* **2000**, *408*, 199.
[33] R. A. Wise, *Nat. Rev. Neurosci.* **2004**, *5*, 483.
[34] W. Cui, M. Li, J. Liu, B. Wang, C. Zhang, L. Jiang, Q. Cheng, *ACS Nano* **2014**, *8*, 9511.
[35] C. Zhu, S. Guo, Y. Fang, S. Dong, *ACS Nano* **2010**, *4*, 2429.
[36] Y. Wang, Y. M. Li, L. H. Tang, J. Lu, J. H. Li, *Electrochem. Commun.* **2009**, *11*, 889.
[37] T. A. Ryan, S. J. Smith, *Neuron* **1995**, *14*, 983.
[38] O. Mashtalir, K. M. Cook, V. N. Mochalin, M. Crowe, M. W. Barsoum, Y. Gogotsi, *J. Mater. Chem. A* **2014**, *2*, 14334.
[39] M. S. Artiles, C. S. Rout, T. S. Fisher, *Adv. Drug Delivery Rev.* **2011**, *63*, 1352.
[40] Y.-R. Kim, S. Bong, Y.-J. Kang, Y. Yang, R. K. Mahajan, J. S. Kim, H. Kim, *Biosens. Bioelectron.* **2010**, *25*, 2366.
[41] Y. Wang, Y. Li, L. Tang, J. Lu, J. Li, *Electrochem. Commun.* **2009**, *11*, 889.
[42] S.-Q. Liu, W.-H. Sun, F.-T. Hu, *Sens. Actuators B: Chem.* **2012**, *173*, 497.
[43] Z.-H. Sheng, X.-Q. Zheng, J.-Y. Xu, W.-J. Bao, F.-B. Wang, X.-H. Xia, *Biosens. Bioelectron.* **2012**, *34*, 125.
[44] M. Naguib, M. Kurtoglu, V. Presser, J. Lu, J. Niu, M. Heon, L. Hultman, Y. Gogotsi, M. W. Barsoum, *Adv. Mater.* **2011**, *23*, 4248.
[45] Q. Tang, Z. Zhou, P. Shen, *J. Am. Chem. Soc.* **2012**, *134*, 16909.
[46] D. Sarkar, W. Liu, X. Xie, A. C. Anselmo, S. Mitragotri, K. Banerjee, *ACS Nano* **2014**, *8*, 3992.
[47] S. Kaech, G. Banker, *Nat. Protoc.* **2006**, *1*, 2406.